ORIGINAL ARTICLE

Noninvasive Imaging Biomarker Identifies Small Airway Damage in Severe Chronic Obstructive Pulmonary Disease

Dragoş M. Vasilescu[1], Fernando J. Martinez[2*], Nathaniel Marchetti[3], Craig J. Galbán[4], Charles Hatt[4,5], Catherine A. Meldrum[4], Chandra Dass[3], Naoya Tanabe[6], Rishindra M. Reddy[4], Amir Lagstein[4], Brian D. Ross[4], Wassim W. Labaki[4], Susan Murray[4*], Xia Meng, Jeffrey L. Curtis[4,7*], Tillie L. Hackett[1], Ella A. Kazerooni[4], Gerard J. Criner[3*], James C. Hogg[1], and MeiLan K. Han[4*]

[1]University of British Columbia, Vancouver, British Columbia, Canada; [2]Weill Cornell Medical College, New York, New York; [3]Lewis Katz School of Medicine, Temple University, Philadelphia, Pennsylvania; [4]University of Michigan, Ann Arbor, Michigan; [5]Imbio, Minneapolis, Minnesota; [6]Kyoto University, Kyoto, Japan; and [7]VA Ann Arbor Healthcare System, Ann Arbor, Michigan

ORCID ID: 0000-0003-3936-4365 (D.M.V.).

Abstract

Rationale: Evidence suggests damage to small airways is a key pathologic lesion in chronic obstructive pulmonary disease (COPD). Computed tomography densitometry has been demonstrated to identify emphysema, but no such studies have been performed linking an imaging metric to small airway abnormality.

Objectives: To correlate *ex vivo* parametric response mapping (PRM) analysis to *in vivo* lung tissue measurements of patients with severe COPD treated by lung transplantation and control subjects.

Methods: Resected lungs were inflated, frozen, and systematically sampled, generating 33 COPD ($n = 11$ subjects) and 22 control tissue samples ($n = 3$ subjects) for micro–computed tomography analysis of terminal bronchioles (TBs; last generation of conducting airways) and emphysema.

Measurements and Main Results: PRM analysis was conducted to differentiate functional small airways disease (PRM^{fSAD}) from emphysema (PRM^{Emph}). In COPD lungs, TB numbers were reduced ($P = 0.01$); surviving TBs had increased wall area percentage ($P < 0.001$), decreased circularity ($P < 0.001$), reduced cross-sectional luminal area ($P < 0.001$), and greater airway obstruction ($P = 0.008$). COPD lungs had increased airspace size ($P < 0.001$) and decreased alveolar surface area ($P < 0.001$). Regression analyses demonstrated unique correlations between PRM^{fSAD} and TBs, with decreased circularity ($P < 0.001$), decreased luminal area ($P < 0.001$), and complete obstruction ($P = 0.008$). PRM^{Emph} correlated with increased airspace size ($P < 0.001$), decreased alveolar surface area ($P = 0.003$), and fewer alveolar attachments per TB ($P = 0.01$).

Conclusions: PRM^{fSAD} identifies areas of lung tissue with TB loss, luminal narrowing, and obstruction. This is the first confirmation that an imaging biomarker can identify terminal bronchial pathology in established COPD and provides a noninvasive imaging methodology to identify small airway damage in COPD.

Keywords: COPD; airways disease; imaging; micro-CT

(Received in original form November 5, 2018; accepted in final form February 21, 2019)

*F.J.M. is Deputy Editor and S.M., J.L.C., G.J.C., and M.K.H. are Associate Editors of *AJRCCM*. Their participation complies with American Thoracic Society requirements for recusal from review and decisions for authored works.

Supported by NIH grants R01 HL122328 (M.K.H.) and K24 HL138188 (M.K.H.); Canadian Thoracic Society and Alpha-1 Foundation fellowships (D.M.V.); Canadian Institutes for Health Research and Michael Smith Foundation for Health Research New Investigator awards (T.L.H.); Merit Review I01 CX000911 from the Department of Veterans Affairs (J.L.C.); National Institute of Allergy and Infectious Diseases grants R01 AI120526 and R21 AI 117371 (J.L.C.); and NIH grant R35 CA197701 (B.D.R.).

Author Contributions: Study was conceived by M.K.H., J.C.H., D.M.V., C.J.G, F.J.M., E.A.K., and B.D.R. Subject recruitment and tissue collection were aided by N.M., C.D., C.A.M., R.M.R., A.L., G.J.C., E.A.K., and M.K.H. Sample and image processing was performed by D.M.V., N.M., C.H., N.T., A.L., J.C.H., C.J.G., B.D.R., and M.K.H. Statistical analysis was performed by D.M.V., S.M., X.M., T.L.H., and M.K.H. Data interpretation and manuscript preparation were performed by all authors previously listed in addition to J.L.C. and W.W.L.

Correspondence and requests for reprints should be addressed to MeiLan K. Han, M.D., M.S., Division of Pulmonary and Critical Care Medicine, University of Michigan, 1500 East Medical Center Drive, 3916 Taubman Center, Ann Arbor, MI 48109. E-mail: mrking@umich.edu.

This article has an online supplement, which is accessible from this issue's table of contents at www.atsjournals.org.

Am J Respir Crit Care Med Vol 200, Iss 5, pp 575–581, Sep 1, 2019

Originally Published in Press as DOI: 10.1164/rccm.201811-2083OC on February 22, 2019
Internet address: www.atsjournals.org

At a Glance Commentary

Scientific Knowledge on the Subject: There is an urgent unmet clinical need to noninvasively detect damage to small airways, a key pathologic lesion in chronic obstructive pulmonary disease (COPD), so that the efficacy of novel therapies can be monitored in real time.

What This Study Adds to the Field: Here we demonstrate that a computed tomography imaging biomarker, parametric response mapping showing functional small airways disease (PRM^{fSAD}), identifies terminal bronchiole loss, luminal narrowing, and obstruction in advanced COPD. These novel findings provide the rationale to test whether high-resolution computed tomography scanning can be used to identify similar small airway lesions in smokers at risk for COPD development.

Chronic obstructive pulmonary disease (COPD) is a highly prevalent disorder with increasing morbidity and mortality (1). Other than smoking cessation, no current therapies can slow disease progression. Highly variable rates of progression (2) and our poor understanding of the factors that influence COPD heterogeneity have impeded development of disease-modifying therapies. Evidence suggests that the numbers of the smallest conducting airways within the lung, termed terminal bronchioles (TBs), are significantly reduced in patients with mild (Global Initiative for Obstructive Lung Disease [GOLD] 1) and moderate (GOLD 2) COPD, before emphysematous destruction (3, 4). Therefore, the ability to assess small airways disease using noninvasive techniques would have the potential to identify patients at the greatest risk for progression to emphysema, where targeted therapies could have a significant impact.

Although thoracic computed tomography (CT) has been shown to correlate with regional lung function (5), reflect regional air content within the lung (6), and quantify emphysema (7, 8) (< -950 Hounsfield units [HU]), imaging the small airways remains more challenging. Current thoracic CT imaging protocols do not permit direct morphometric analysis of the terminal bronchioles, which are generally less than 0.5 mm in diameter. Indirect assessment of small airways disease using clinical CT has been attempted via density measures of "air trapping," using quantification of voxels less than -856 HU on expiratory CT (9, 10). However, none of these attempts to quantify small airway abnormalities have been validated in relationship to pathologic abnormalities of human lung tissue.

Recently, Galbán and colleagues developed an imaging biomarker, parametric response mapping (PRM), for precise voxel-based classification of lung density (11). This technique identifies lung regions as normal (PRM^{Norm}), emphysematous (PRM^{Emph}), and nonemphysematous gas trapping (PRM^{fSAD}) using dynamic image registration to identify changes in voxel density between inspiration and expiration. Such nonemphysematous gas trapping was conservatively interpreted to be a functional change of the small airways that might reflect a variety of pathological changes, and hence was termed "functional small airways disease" (fSAD) (11). Longitudinal imaging studies suggest PRM^{fSAD} can be detected in mild (GOLD 1) and moderate (GOLD 2) COPD, followed by the later development of emphysema, and is associated with subsequent lung function decline even among at-risk individuals initially without airflow obstruction (12).

The goal of the current study was to define the nature of small airway damage identified by PRM^{fSAD} using human lung tissue from individuals with and without COPD. We used ultra-high-resolution micro-CT analysis of the *ex vivo* lung to quantify small airways and parenchymal structures and relate those measurements to *in vivo* thoracic CT scans obtained before lung removal. Portions of these analyses have previously been presented in abstract form (13–15).

Methods

Patient Cohort

Informed consent was obtained from 11 subjects with end-stage COPD treated by lung transplantation and from the next of kin of three donor control subjects through the Gift of Life program, under institutional review board–approved protocols at the University of Michigan and Temple University. The demographic and clinical characteristics of all donors are presented in Table 1.

In Vivo PRM Analysis

We acquired CT images and analyzed tissue samples using a systematic workflow outlined in Figure 1. First, inspiratory and expiratory multidetector volumetric CT scans were performed *in vivo* on subjects with COPD before treatment by lung transplantation or donor control subjects before lung harvesting. The CT scans were obtained at 120 kVP, 120 mAs, with a 0.625-mm slice thickness. PRM analysis was performed using the Lung Density Analysis software package (Imbio, LLC) as previously described (12, 16). This analysis enabled each voxel within the registered inspiratory and expiratory CT scans to be classified as PRM^{Norm} ($\geqslant -950$ HU at inspiration and $\geqslant -856$ HU at expiration, green), PRM^{fSAD} ($\geqslant -950$ HU at inspiration and < -856 HU at expiration, yellow), or PRM^{Emph} (< -950 HU at inspiration and < -856 HU at expiration, red) (8, 17–19). PRM data were expressed as a percentage of total lung volume (sum of all voxels within the lung segmentation).

Sampling of the *Ex Vivo* Lung

Intact explanted lung specimens were inflated with air to a transpulmonary pressure of 30 cm H_2O, then deflated and held at 10 cm H_2O while frozen using liquid nitrogen vapor (Figure 1). To estimate total lung volume before sampling and for later identification of the resection sample on the preoperative scan, frozen lung explants were CT scanned at 120 kVP, 120 mAs, and 0.625-mm slice thickness. While still frozen, the lung explant was cut into contiguous 2-cm-thick slices in the transaxial plane, as previously described (3, 20). For the three control subjects, to avoid sampling bias, we used a systematic uniform random (SUR) sampling design to obtain a total of 22 representative cylindrical tissue cores measuring 1.5 cm in diameter by following the guidelines of the American Thoracic Society and European Respiratory Society guidelines for stereology (21). In contrast, as pathology within the COPD lungs was not uniformly distributed because of the intrinsic nature of this disease, for the COPD lungs we used a targeted sampling approach to generate 33 tissue cores obtained from regions of lung affected by PRM^{Emph} and PRM^{fSAD}.

Table 1. Demographics and Pulmonary Function Data on Participants Supplying Lung Samples

	Control	COPD
Lung specimen used, right/left	3/0	5/6
No. of samples	22	33
No. of airways segmented	45	44
Age, yr*	51.33 ± 19.40	62.55 ± 3.33
Sex, F/M	1/2	5/6
Body height, cm	176.55 ± 1.77	171.67 ± 11.52
Weight, kg	110.40 ± 35.01	72.91 ± 20.81
Race	2 white; 1 African American	9 white; 1 African American; 1 Native American
Smoking history, pack-years	0	50.57 ± 14.14
FEV_1, L	NA	0.62 ± 0.15
FEV_1% predicted	NA	22.00 ± 4.31
FVC, L	NA	2.17 ± 0.59
FVC% predicted	NA	52.55 ± 7.42
FEV_1/FVC	NA	0.29 ± 0.06
$FEF_{25–75}$	NA	0.22 ± 0.04

Definition of abbreviations: COPD = chronic obstructive pulmonary disease; $FEF_{25–75}$ = forced expiratory flow, midexpiratory phase; NA = not applicable.
Data are mean ± SD, unless specified.
*Indicates significance at $P < 0.01$.

By registering each preoperative *in vivo* thoracic CT scan with each explanted *ex vivo* lung specimen CT scan, as previously described (22), it was possible to differentiate the areas of lung classified as PRM^{fSAD} and PRM^{Emph}, which guided our sampling. A localized PRM measurement for the core was then calculated from the preoperative *in vivo* CT scan.

Micro-CT Imaging and Morphometric Assessment of the *Ex Vivo* Lung Cores

Tissue cores were scanned frozen at −30°C by a previously developed cryo-stage and imaging protocol (23), using a Nikon HMX 225ST micro-CT scanner (40 kV, 350 μA, 500 ms exposure time) and were reconstructed with an isotropic voxel size of 11 μm^3.

We identified TBs within the micro-CT scans of the cores by following consecutive airway branches until reaching the first generation of respiratory bronchioles, termed transitional bronchioles (TrBs) (24), which were distinguished based on the first occurrence of individual alveoli along the airway wall. Identification of TrBs is critical for unambiguous identification of the transition from the conducting to the respiratory zone in the airway tree, which enabled us, by dividing the number of respective bronchioles by the sample volume, to enumerate (per milliliter of lung) TBs per milliliter and obstructed TBs (defined as 100% lumen obstruction/closure) per milliliter (4, 21).

TB morphometry from the micro-CT scans of the cores was assessed using methods developed by Tanabe and colleagues (25, 26). Briefly, we used 10 cross-sectional SUR distributed images through each TB segmentation to calculate the branch length and the average luminal cross-sectional area, average wall thickness, wall area, wall area percentage, circularity, and number of alveolar attachments per TB.

To calculate mean airspace size (mean linear intercept, Lm) and alveolar surface area for each tissue core, we captured 10 SUR images throughout the entire micro-CT scan, using custom software specifically designed for stereological counting on micro-CT images (Computer Assisted Stereology) developed in the Hogg laboratory, implemented in Matlab (Mathworks). A line grid (1-mm-long lines in a checkered pattern) was overlaid on each of the 10 SUR images per sample to determine the number of intercepts between alveolar septum and each line, and the endpoints of each line were used to determine the volume fraction of alveolar tissue. Combining the tissue volume fraction with the sample volume and the alveolar surface density permitted an estimate of alveolar surface area per tissue sample. The assessment of Lm and alveolar surface area with micro-CT has been

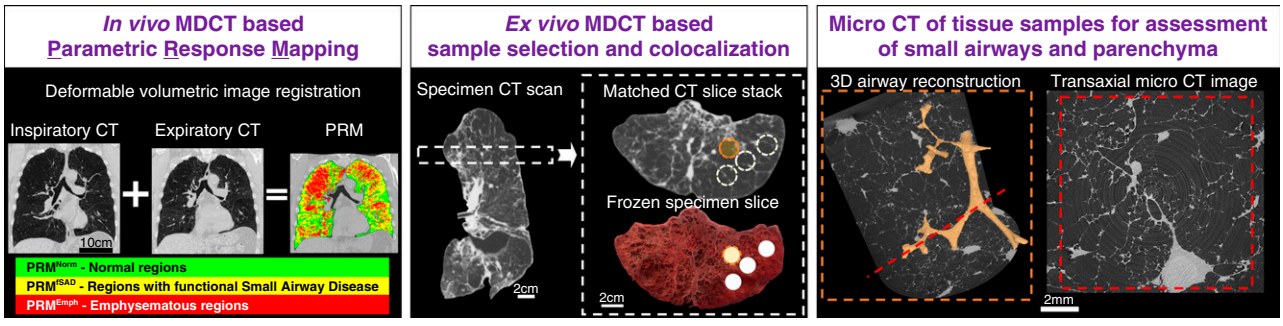

Figure 1. Overview of image acquisition and tissue processing. Left panel: parametric response mapping (PRM) analysis was performed on *in vivo* thoracic computed tomography (CT) scans, classifying each voxel of lung into one of three classes: normal (PRM^{Norm}), functional small airways disease (PRM^{fSAD}), and emphysema (PRM^{Emph}). Middle panel: after lungs were removed, each explanted lung specimen was first air inflated and frozen to enable *ex vivo* scanning with a CT scanner. Subsequently, the lung specimen was cut into 2-cm slices, from which tissue cores were extracted for micro-CT imaging. The micro-CT scans enabled a detailed assessment of small airway morphometry and alveolar destruction. Right panel: finally, sample core locations were matched back to the preoperative *in vivo* CT scan to enable a correlation between the morphometric parameters and the PRM classification. 3D = three-dimensional; MDCT = multidetector CT.

validated by multiple studies (4, 21, 27, 28). Number of TBs per milliliter, number of obstructed TBs per milliliter, airspace size (Lm), and alveolar surface area were expressed as one measure per tissue core. The TB morphometry (branch length, cross-sectional lumen area, wall area percentage, and circularity) was measured in multiple TBs per core.

Statistical Analysis

Differences between whole-lung PRM metrics in control subjects versus subjects with COPD were assessed using two sample *t* tests. Differences in morphometric parameters measured by micro-CT and local PRM classifications between control and COPD tissue samples were assessed using linear mixed regression models assuming Gaussian distribution to account for various sources of correlation in the data given multiple measures per subject using SAS version 9.4 (SAS Institute Inc., Cary, NC, USA). To account for multiple cores per subject and multiple measures per core, we used nested linear mixed-effect models where there were multiple measures per core (cross-sectional lumen area, wall area percentage, and circularity) and nonnested linear mixed-effect models for parameters where there was only one measurement per core (TBs per milliliter, number of obstructed TBs per milliliter of lung, Lm, and alveolar surface area). This regression methodology was also used for multivariable modeling to determine the relationship between PRM^{fSAD} or PRM^{Emph} and micro-CT measures of interest treated as outcomes. Figures were created using R 2018 (R Foundation for Statistical Computing, Vienna, Austria).

Results

Patient Demographics

This analysis was conducted using 33 samples from a total of 11 lungs from patients with GOLD 4 COPD undergoing lung transplantation (mean, 3 cores per subject; 95% confidence interval, 2.59–3.41), and 22 samples from three control donor lungs (mean, 7.3 cores per subject; 95% confidence interval, 6.94–7.72). Patients with COPD were significantly older, and they had a substantial smoking history (50.57 pack-years) compared with the control donors, who were all never-smokers (Table 1). Lung function data were unavailable for the control donors.

Whole Lung and Localized PRM Analysis

In vivo PRM analysis identified on average 42.65% PRM^{fSAD} ($P < 0.001$) and 30.68% PRM^{Emph} ($P < 0.001$) in GOLD 4 COPD lungs; control lungs had no emphysema and 15.63% PRM^{fSAD} (*see* Table E1 in the online supplement). After lung sampling, the exact tissue sample locations were mapped back to the *in vivo* CT to perform a localized PRM analysis for each tissue sample (Figure E1). This localized PRM analysis demonstrated that, compared with controls, GOLD 4 COPD tissue samples predominantly contained 49.38% PRM^{fSAD} ($P < 0.001$), with only 20.91% PRM^{Norm} ($P < 0.001$) and 28.41% PRM^{Emph} ($P < 0.001$) (Table E1). Representative micro-CT analyses and corresponding PRM values are shown in Figure 2.

Regression Analysis of Micro-CT Morphometry and Localized PRM Analysis

Using regression analyses, we found a unique relationship between PRM^{fSAD} and an increased number of obstructed TBs per milliliter ($P = 0.008$), decreased TB cross-sectional lumen area ($P < 0.001$), and decreased circularity ($P < 0.001$) (Table 2). PRM^{Emph} correlated uniquely with airspace size (Lm, $P < 0.001$), alveolar surface area ($P = 0.003$), and the number of alveolar attachments per TB ($P = 0.01$). Scatter plots for these relationships are displayed in Figure E2. The number of TBs per milliliter of lung and wall area percentage correlated with both PRM^{fSAD} and PRM^{Emph}.

To further visualize the relationship of small airway abnormalities with PRM^{fSAD} and PRM^{Emph}, we plotted the number of TBs versus airspace size (Lm) for each individual lung sample, which was then color coded based on their dominant (≥33.3%) PRM classification (PRM^{Norm} [green], PRM^{fSAD} [yellow], or PRM^{Emph} [red]) (Figure 3). The 5th to 95th percentiles (339.61–397.87 μm) of Lm for control samples are shown to demonstrate the normal range of airspace sizes. The majority (73.7%) of COPD lung samples that were dominant for PRM^{fSAD} had

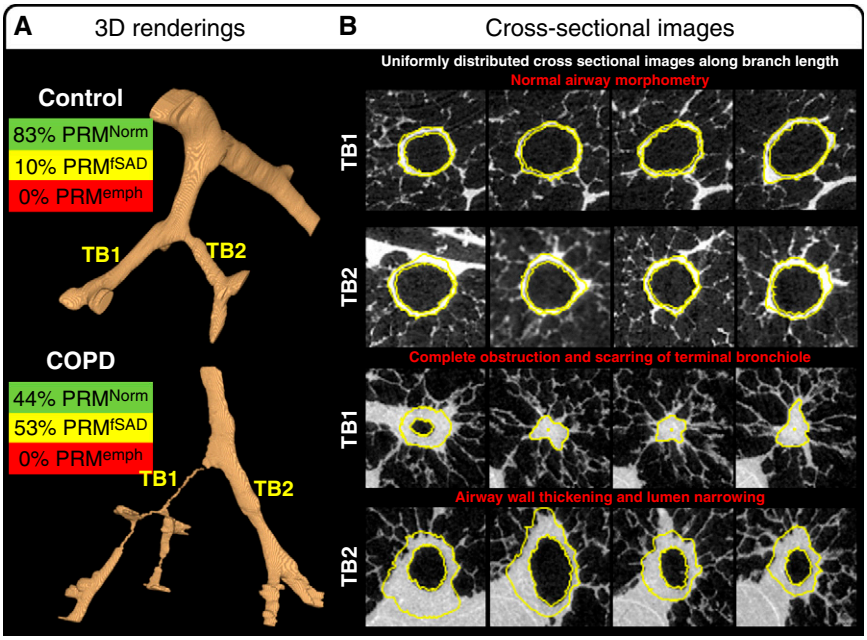

Figure 2. Three-dimensional (3D) renderings of representative small airway trees present in tissue samples extracted from control subjects and patients with chronic obstructive pulmonary disease (COPD). (*A*) Representative 3D segmentation of all visible airways within a control and COPD sample are provided in addition to the matched parametric response mapping (PRM) analysis from the *ex vivo* computed tomography scan. (*B*) The cross-sectional images along the terminal bronchiole (TB) branch length demonstrate normal airway morphology in TB1 and 2 of the control sample compared with the COPD sample, which demonstrates complete obstruction and scarring in TB1 and airway wall thickening and lumen narrowing in TB2. Yellow lines indicate the inner and outer wall segmentations used for the calculations of luminal cross-sectional area, inner and outer wall perimeter, wall thickness, and wall area percentage. Cross-sectional images are 900 μm wide. emph = emphysema; fSAD = functional small airways disease; Norm = normal.

Table 2. Regression Analysis Parameter Estimates Demonstrating the Relationships between Localized Parametric Response Mapping Classification and Micro–Computed Tomography Morphometry

Measurements	PRM^{fSAD}			PRM^{Emph}		
	Estimate	SE	*P* Value	Estimate	SE	*P* Value
Terminal bronchiole morphometry						
Terminal bronchioles per ml of lung	−0.007	0.003	**0.02**	−0.008	0.004	**0.03**
No. of obstructed bronchioles per ml of lung	0.004	0.002	**0.008**	0.00	0.002	0.99
Cross-sectional lumen area, mm^2	−0.004	0.001	**<0.001**	−0.001	0.002	0.23
Wall area percentage	0.50	0.07	**<0.001**	0.33	0.10	**0.002**
Circularity	−0.001	0.0003	**<0.001**	−0.0007	0.0004	0.09
Alveolar attachment number per terminal bronchiole	−0.007	0.006	0.25	−0.02	0.009	**0.01**
Parenchymal morphometry						
Mean linear intercept, μm	2.17	1.70	0.20	15.08	2.53	**<0.001**
Alveolar surface area, cm^2/ml	−0.02	0.08	0.81	−0.17	0.06	**0.003**

Definition of abbreviations: Emph = emphysema; fSAD = functional small airways disease; PRM = parametric response mapping.
Bold indicates $P < 0.05$.

a significantly reduced number of TBs and an Lm value greater than the 95th percentile of controls. In contrast, most (64.3%) COPD lung samples that were PRM^{Emph} dominant had the same reduction in TB number but had an Lm greater than 1,000 μm, which is the lower limit of resolution for clinical CT and therefore presents as detectable emphysematous disease.

Micro-CT Assessment of Small Airways Disease and Emphysema

When assessing small airways disease using micro-CT (Table E1), compared with control lungs, GOLD 4 COPD lungs had significantly fewer TBs (0.71 TB/ml vs. 1.94 TB/ml; $P = 0.01$). Furthermore, the remaining TBs in subjects with COPD were obstructed (0.45 per ml of lung vs. 0; $P < 0.001$), with decreased cross-sectional area (0.11 vs. 0.33 mm^2; $P < 0.001$), decreased circularity (0.81 vs. 0.88; $P < 0.001$), increased wall area percentage (71.81 vs. 36.83; $P < 0.001$), and reduced number of alveolar attachments per TB (3.51 vs. 4.56; $P = 0.004$) (Table E1). When assessing emphysema compared with controls, COPD lungs had a significant increase in airspace size (1,078.42 vs. 366.16 μm; $P < 0.001$). This finding is in line with a significant decrease in alveolar surface area in COPD samples (12.36 vs. 50.65 cm^2/ml; $P < 0.001$) (Table E1).

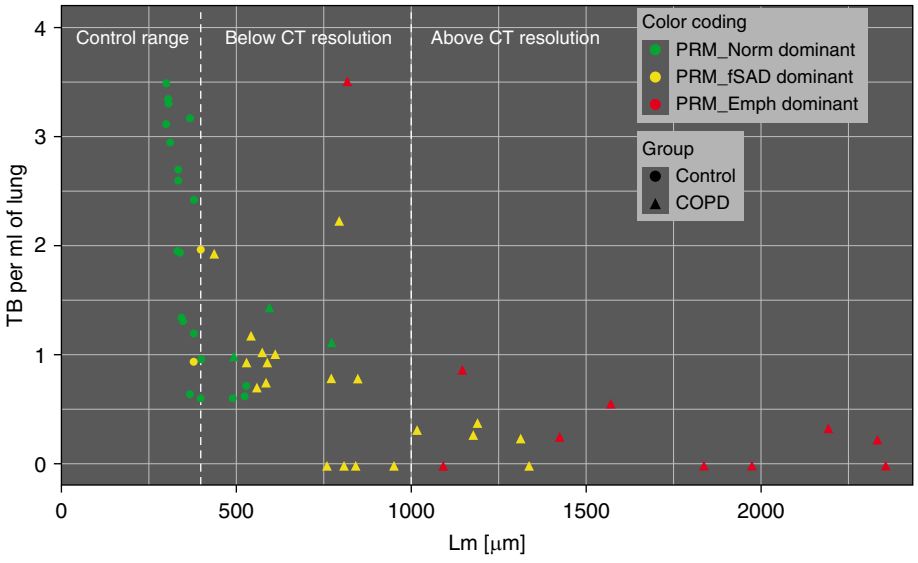

Figure 3. Relationship between parametric response mapping (PRM) classification, number of terminal bronchioles (TBs), and airspace size. Samples are color coded based on predominant PRM abnormality (≥33.3%) PRM^{Norm} (normal; green), PRM^{fSAD} (functional small airways disease; yellow), or PRM^{Emph} (emphysema; red), and by specimen type (control, circle; chronic obstructive pulmonary disease [COPD], triangle). Plot demonstrates that the majority of COPD lung samples dominant for PRM^{fSAD} had significantly reduced number of TBs and a mean linear intercept (Lm) value greater than the 95th percentile of controls. COPD lung samples that were PRM^{Emph} dominant had similar reduction in TB number but Lm greater than 1,000 μm, which is the lower limit of resolution for clinical computed tomography (CT) and therefore presents as detectable emphysematous disease.

Discussion

This study, to our knowledge, provides the first direct evidence using micro-CT that the thoracic CT biomarker PRM^{fSAD} correlates in COPD with both loss of TBs and with narrowing, thickening, and obstruction of surviving TBs. Furthermore, we show that the PRM^{Emph} biomarker correlates in COPD with enlarged airspace size, decreased alveolar surface area, and loss of TB alveolar attachments. These results strongly support the hypothesis that PRM^{fSAD} and PRM^{Emph} are clinically available CT biomarkers that can be used to noninvasively assess small airways disease and emphysema in COPD.

Almost 50 years ago, Mead wrote an editorial that referred to the small airways less than 2 mm in diameter as a quiet zone within the lungs (29). Disease can accumulate over many years without being noticed, because in control subjects and

control postmortem lungs, the small airways contribute minimally to total resistance to airflow; their large numbers and parallel arrangement means that a 50% reduction in their number would be required to double the resistance to airflow. Thus, Mead proposed that small airways disease could develop over time without being detected using spirometry (29). In support of this hypothesis, our previous PRM analyses found that even in smokers without airflow obstruction, PRM^{fSAD}, which we demonstrate here to correlate with pathological small airway changes, identifies individuals at increased risk for FEV_1 decline (12). Furthermore, in longitudinal studies of patients with mild (GOLD 1) and moderate (GOLD 2) COPD, voxels identified as PRM^{fSAD} transitioned into PRM^{Emph} over time (16).

In this study, using ultra-high-resolution micro-CT, we confirmed previous findings (3, 4, 26) that TBs are extensively lost in severe COPD but also demonstrate that surviving TBs are extensively remodeled, leading to small airway narrowing and obstruction compared with control donors. Importantly, these new data validate that PRM^{fSAD} is a sensitive imaging biomarker that correlates with remodeling of surviving TBs that have thickened walls, decreased circularity, and narrowed or obstructed lumens even in areas without measurable emphysema by micro-CT. Such changes in airway morphometry would clearly affect airflow and relate to the nonemphysematous gas trapping detectable by PRM^{fSAD}. In contrast, PRM^{Emph} correlated with increased airspace size, decreased alveolar surface area, and loss of TB alveolar attachments, which confirms and extends prior studies demonstrating that a density threshold less than −950 HU correlates with increased airspace size measured by histology (4, 8, 18). In support of this finding, Kirby and colleagues recently reported that total airway count on the basis of CT negatively correlates with PRM^{fSAD} but not PRM^{Emph} (30).

Interestingly, TB numbers and wall area percentage correlated with both PRM^{fSAD} and PRM^{Emph}. Because Koo and colleagues (4) previously demonstrated that TBs are lost before alterations in alveolar surface area, and Hogg and colleagues (20) showed that small airways in patients with COPD have thickened walls, we expected that loss of TB and wall area percentage would correlate with both PRM metrics. Admittedly, we have a tripartite classification system to describe what is likely a continuous process of transition from small airway damage to emphysematous tissue destruction. Hence, it is not surprising that the PRM^{Emph} classification may also identify regions in transition to emphysema.

Although we validate the capability of PRM^{fSAD} to identify small airways disease in severe COPD, further validation for PRM^{fSAD} to detect preclinical disease in at-risk smokers is imperative in light of recent studies (31). If further validated, PRM analysis could become a useful noninvasive biomarker to detect the earliest pathological changes in COPD and be an outcome measure for therapies designed to block transition from small airways disease to emphysema. Nonetheless, on the basis of the validation provided here, the PRM classification for nonemphysematous air trapping termed "fSAD" is clearly correlated with small airway remodeling, even in areas of lung tissue without significant emphysema. Therefore, we propose that the name of this classification be changed from "functional small airways disease," which was determined based on the interpretation of the CT data, to simply "small airways disease" (i.e., PRM^{SAD}).

The strengths of this analysis include experiments conducted on whole human lungs from patients with very severe COPD and donor control subjects. Nevertheless, the study has limitations. A relatively small number of explanted lungs were studied because of the intense rigor required to obtain paired inspiratory and expiratory CT imaging before lung transplantation surgery. Thus, the lungs we examined may not be representative of all patients with very severe COPD. To attempt to minimize this limitation, we systematically examined areas of lung containing varying levels of structural abnormality to understand the relationship between small airways disease and emphysema. Given that we required whole lungs from healthy donors, we also did not have lung function data available on the control subjects, although CT metrics supported that the lungs were indeed healthy. Furthermore, this cross-sectional study does not permit observation of disease progression over time or determining if patients with COPD may have been born with a reduced number of airways. Despite these limitations, the numbers of TBs and alveolar surface area reported for the donor control subjects in this study are consistent with those previously reported in studies of the normal human lung (24, 32). As we only analyzed TB morphometry, therefore, we cannot conclude that PRM^{SAD} identifies small airways disease in all small conducting airways. Last, although our prior clinical and imaging studies demonstrate PRM^{SAD} precedes the development of PRM^{Emph} and identifies patients at risk for more rapid decline (12), this study does not examine tissue from "early" disease, as whole lungs from patients with minimal disease are not typically resected. Therefore, we cannot confirm the type of histologic abnormality identified by PRM^{SAD} in mild- and moderate-stage disease. Developing techniques to correlate micro-CT to *in vivo* imaging using smaller amounts of tissue, such as whole lung lobes removed for clinically indicated resections, will be required to validate PRM^{SAD} in patients with less severe disease.

In conclusion, we demonstrate that the noninvasive CT biomarkers PRM^{SAD} and PRM^{Emph} strongly correlate with anatomic small airways disease and emphysema, respectively, in severe COPD. Our investigative group is working on developing additional techniques to elucidate the nature of small airway abnormality identified by PRM in patients with milder disease. ■

Author disclosures are available with the text of this article at www.atsjournals.org.

References

1. Rabe KF, Hurd S, Anzueto A, Barnes PJ, Buist SA, Calverley P, *et al.*; Global Initiative for Chronic Obstructive Lung Disease. Global strategy for the diagnosis, management, and prevention of chronic obstructive pulmonary disease: GOLD executive summary. *Am J Respir Crit Care Med* 2007;176:532–555.
2. Vestbo J, Edwards LD, Scanlon PD, Yates JC, Agusti A, Bakke P, *et al.*; ECLIPSE Investigators. Changes in forced expiratory volume in 1 second over time in COPD. *N Engl J Med* 2011;365:1184–1192.

3. McDonough JE, Yuan R, Suzuki M, Seyednejad N, Elliott WM, Sanchez PG, *et al*. Small-airway obstruction and emphysema in chronic obstructive pulmonary disease. *N Engl J Med* 2011;365:1567–1575.
4. Koo HK, Vasilescu DM, Booth S, Hsieh A, Katsamenis OL, Fishbane N, *et al*. Small airways disease in mild and moderate chronic obstructive pulmonary disease: a cross-sectional study. *Lancet Respir Med* 2018; 6:591–602.
5. Hoffman EA, Simon BA, McLennan G. State of the Art: a structural and functional assessment of the lung via multidetector-row computed tomography: phenotyping chronic obstructive pulmonary disease. *Proc Am Thorac Soc* 2006;3:519–532.
6. Hoffman EA. Effect of body orientation on regional lung expansion: a computed tomographic approach. *J Appl Physiol (1985)* 1985;59: 468–480.
7. Coxson HO, Mayo JR, Behzad H, Moore BJ, Verburgt LM, Staples CA, *et al*. Measurement of lung expansion with computed tomography and comparison with quantitative histology. *J Appl Physiol (1985)* 1995;79:1525–1530.
8. Gevenois PA, De Vuyst P, de Maertelaer V, Zanen J, Jacobovitz D, Cosio MG, *et al*. Comparison of computed density and microscopic morphometry in pulmonary emphysema. *Am J Respir Crit Care Med* 1996;154:187–192.
9. Jain N, Covar RA, Gleason MC, Newell JD Jr, Gelfand EW, Spahn JD. Quantitative computed tomography detects peripheral airway disease in asthmatic children. *Pediatr Pulmonol* 2005;40:211–218.
10. Matsuoka S, Kurihara Y, Yagihashi K, Hoshino M, Watanabe N, Nakajima Y. Quantitative assessment of air trapping in chronic obstructive pulmonary disease using inspiratory and expiratory volumetric MDCT. *AJR Am J Roentgenol* 2008;190:762–769.
11. Galbán CJ, Han MK, Boes JL, Chughtai KA, Meyer CR, Johnson TD, *et al*. Computed tomography-based biomarker provides unique signature for diagnosis of COPD phenotypes and disease progression. *Nat Med* 2012;18:1711–1715.
12. Bhatt SP, Soler X, Wang X, Murray S, Anzueto AR, Beaty TH, *et al*.; COPDGene Investigators. Association between functional small airway disease and FEV1 decline in chronic obstructive pulmonary disease. *Am J Respir Crit Care Med* 2016;194:178–184.
13. Vasilescu DM, Marchetti N, Galbán CJ, Meldrum C, Ross BD, Martinez CH, *et al*. The relationship between functional small airways disease and small airways pathology in COPD [abstract]. *Am J Respir Crit Care Med* 2017;195:A157.
14. Vasilescu DM, Marchetti N, Galbán C, Heist K, Meldrum C, Reddy R, *et al*. MDCT parametric response mapping identifies loss of lung terminal bronchioles in COPD. *Eur Respir J* 2017;50:PA803.
15. Vasilescu DM, Marchetti N, Galbán C, Meldrum CA, Reddy RM, Lagstein A, *et al*. Multi-detector computed tomography based parametric response mapping correlates with small airway remodeling in COPD [abstract]. *Am J Respir Crit Care Med* 2018;197: A1036.
16. Labaki W, Gu T, Murray S, Hatt CR, Galban CJ, Ross BD, *et al*. Five-year parametric response mapping changes in chest computed tomography of smokers in the COPDGene cohort. *Acad Radiol* 2019; 26:217–223.
17. Regan EA, Hokanson JE, Murphy JR, Make B, Lynch DA, Beaty TH, *et al*. Genetic epidemiology of COPD (COPDGene) study design. *COPD* 2010;7:32–43.
18. Gevenois PA, de Maertelaer V, De Vuyst P, Zanen J, Yernault JC. Comparison of computed density and macroscopic morphometry in pulmonary emphysema. *Am J Respir Crit Care Med* 1995;152: 653–657.
19. Newman KB, Lynch DA, Newman LS, Ellegood D, Newell JD Jr. Quantitative computed tomography detects air trapping due to asthma. *Chest* 1994;106:105–109.
20. Hogg JC, Chu F, Utokaparch S, Woods R, Elliott WM, Buzatu L, *et al*. The nature of small-airway obstruction in chronic obstructive pulmonary disease. *N Engl J Med* 2004;350:2645–2653.
21. Hsia CC, Hyde DM, Ochs M, Weibel ER; ATS/ERS Joint Task Force on Quantitative Assessment of Lung Structure. An official research policy statement of the American Thoracic Society/European Respiratory Society: standards for quantitative assessment of lung structure. *Am J Respir Crit Care Med* 2010; 181:394–418.
22. Verleden SE, Vos R, Vandermeulen E, Ruttens D, Bellon H, Heigl T, *et al*. Serial parametric response mapping to diagnose bronchiolitis obliterans syndrome. *Am J Transplant* 2016;16:3262–3269.
23. Vasilescu DM, Phillion AB, Tanabe N, Kinose D, Paige DF, Kantrowitz JJ, *et al*. Nondestructive cryomicro-CT imaging enables structural and molecular analysis of human lung tissue. *J Appl Physiol (1985)* 2017;122:161–169.
24. Haefeli-Bleuer B, Weibel ER. Morphometry of the human pulmonary acinus. *Anat Rec* 1988;220:401–414.
25. Tanabe N, Vasilescu DM, McDonough JE, Kinose D, Suzuki M, Cooper JD, *et al*. Micro-computed tomography comparison of preterminal bronchioles in centrilobular and panlobular emphysema. *Am J Respir Crit Care Med* 2017;195:630–638.
26. Tanabe N, Vasilescu DM, Kirby M, Coxson HO, Verleden SE, Vanaudenaerde BM, *et al*. Analysis of airway pathology in COPD using a combination of computed tomography, micro-computed tomography and histology. *Eur Respir J* 2018;51:1701245.
27. Vasilescu DM, Klinge C, Knudsen L, Yin L, Wang G, Weibel ER, *et al*. Stereological assessment of mouse lung parenchyma via nondestructive, multiscale micro-CT imaging validated by light microscopic histology. *J Appl Physiol (1985)* 2013;114:716–724.
28. Scott AE, Vasilescu DM, Seal KA, Keyes SD, Mavrogordato MN, Hogg JC, *et al*. Three dimensional imaging of paraffin embedded human lung tissue samples by micro-computed tomography. *PLoS One* 2015;10:e0126230.
29. Mead J. The lung's "quiet zone". *N Engl J Med* 1970;282:1318–1319.
30. Kirby M, Tanabe N, Tan WC, Zhou G, Obeidat M, Hague CJ, *et al*.; CanCOLD Collaborative Research Group; Canadian Respiratory Research Network; CanCOLD Collaborative Research Group, the Canadian Respiratory Research Network. Total airway count on computed tomography and the risk of chronic obstructive pulmonary disease progression: findings from a population-based study. *Am J Respir Crit Care Med* 2018;197:56–65.
31. Martinez FJ, Han MK, Allinson JP, Barr RG, Boucher RC, Calverley PMA, *et al*. At the root: defining and halting progression of early chronic obstructive pulmonary disease. *Am J Respir Crit Care Med* 2018;197:1540–1551.
32. Wiebe BM, Laursen H. Lung morphometry by unbiased methods in emphysema: bronchial and blood vessel volume, alveolar surface area and capillary length. *APMIS* 1998;106:651–656.